Protein Science (1996), 5:1963–1972. Cambridge University Press. Printed in the USA.

High-resolution structures of the bifunctional enzyme and transcriptional coactivator DCoH and its complex with a product analogue

JEFF D. CRONK, JAMES A. ENDRIZZI, AND TOM ALBER

Department of Molecular and Cell Biology, University of California at Berkeley, Berkeley, California 94720-3206

(RECEIVED May 2, 1996; ACCEPTED July 23, 1996)

Abstract

DCoH, the dimerization cofactor of hepatocyte nuclear factor 1 (HNF-1), functions as both a transcriptional coactivator and a pterin dehydratase. To probe the relationship between these two functions, the X-ray crystal structures of the free enzyme and its complex with the product analogue 7,8-dihydrobiopterin were refined at 2.3 Å resolution. The ligand binds at four sites per tetrameric enzyme, with little apparent conformational change in the protein. Each active-site cleft is located in a subunit interface, adjacent to a prominent saddle motif that has structural similarities to the TATA binding protein. The pterin binds within an arch of aromatic residues that extends across one dimer interface. The bound ligand makes contacts to three conserved histidines, and this arrangement restricts proposals for the enzymatic mechanism of dehydration. The dihedral symmetry of DCoH suggests that binding to the dimerization domain of HNF-1 likely involves the superposition of two-fold rotation axes of the two proteins.

Keywords: dehydratase; enzyme mechanism; gene regulation; transcriptional coactivator

The bifunctional protein DCoH is both a transcriptional coactivator and a metabolic enzyme. Cotransfection experiments in different cell lines indicate that DCoH stimulates expression of genes controlled by the homeodomain-containing, hepatocyte nuclear factor-1 (HNF-1) family of transcriptional activators (Mendel et al., 1991; von Strandmann & Ryffel, 1995). Like most coactivators, however, DCoH does not bind DNA. Consequently, protein–protein interactions may be central to the coactivator function.

Consistent with this model, DCoH purified from rat liver nuclear extracts is found in a 2:2 complex with HNF-1α (Mendel et al., 1991). HNF-1 proteins form dimers by virtue of a 32-amino acid, helical dimerization domain that is necessary and sufficient for interaction with DCoH (De Francesco et al., 1991; Mendel et al., 1991; Pastore et al., 1992; Hansen, 1994). In addition, DCoH localizes to nuclei early in *Xenopus* development, when HNF-1 proteins are absent (von Strandmann & Ryffel, 1995). These results support the suggestion that DCoH may stimulate gene expression by enhancing the dimerization and stability of HNF-1 proteins (Hansen & Crabtree, 1993) or other potential targets. Alternatively, DCoH may bind to other components of the transcription complex or to the products of target genes.

Although the mechanism of transcriptional coactivation by DCoH has not been established, the metabolic roles of the protein are better defined. Originally identified as a phenylalanine hydroxylase stimulator protein, DCoH was shown to catalyze dehydration of a 4a-carbinolamine form of the biopterin cofactor used by the aromatic amino acid hydroxylases and NO synthase (Kaufman, 1970, 1993). The pterin-4a-carbinolamine dehydratase (PCD) activity of DCoH, in concert with the enzyme dihydropteridine reductase, regenerates the active, reduced form of the cofactor (Fig. 1A). The pterin-4a-carbinolamine dehydrates spontaneously in aqueous solution, but at rates too slow to support the maximum turnover rate of phenylalanine hydroxylase. In coupled assays of phenylalanine hydroxylase activity, the presence of DCoH stimulates the production of tyrosine at least eightfold (Huang & Kaufman, 1973; Köster et al., 1995), and direct measurements of k_{cat}/k_{uncat} for the dehydratase reaction have yielded values as high as 2,000 (Rebrin et al., 1995).

In vivo, the DCoH-catalyzed dehydration reaction appears to prevent spontaneous rearrangements of the pterin-4a-carbinolamine, which produce 7-substituted pterins (Curtius et al., 1990; Davis et al., 1991). Consistent with this idea, nonsense and missense mutations in DCoH genes have been identified in patients who have elevated levels of phenylalanine and excrete large amounts of 7-substituted pterins (Citron et al., 1993). The ability of DCoH to block rearrangements of the pterin cofactor may be functionally as important as the stimulation of aromatic amino acid hydroxylase enzymes (Davis et al., 1992).

Little is known about the relationship between the enzymatic and coactivator functions of DCoH. Conformational polymor-

Reprint requests to: Tom Alber, Department of Molecular and Cell Biology, 229 Stanley Hall #3206, University of California, Berkeley, California 94720-3206; e-mail: tom@ucxray6.berkeley.edu.

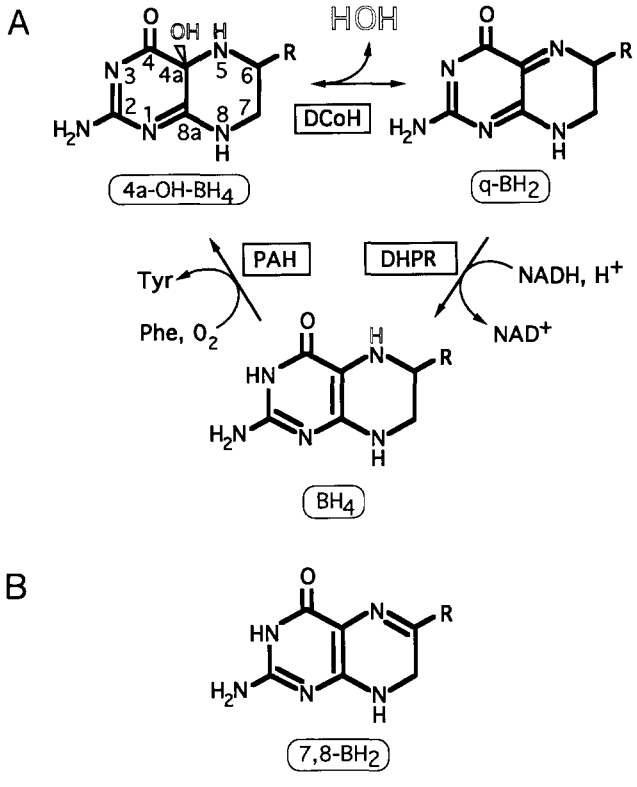

Fig. 1. A: Metabolic cycle involving DCoH. DCoH catalyzes dehydration of a pterin-4a-carbinolamine cofactor, converting 4a-hydroxytetrahydrobiopterin (4a-OH-BH_4) to quinoid dihydrobiopterin (q-BH_2). The q-BH_2 is reduced by dihydropteridine reductase (DHPR) and the product, tetrahydrobiopterin (BH_4), is used by the aromatic amino acid hydroxylases [e.g., phenylalanine hydroxylase (PAH)]. Names of pterin substrates are enclosed in ovals; enzymes are in boxes. The numbering system for pterins is shown for 4a-OH-BH_4. **B:** Structure of the product analogue 7,8-dihydrobiopterin (7,8-BH_2). R, dihydroxypropyl.

phism may be important for these activities, because the catalytically active form of the protein is tetrameric, whereas complexes with HNF-1 are heterotetramers (Huang et al., 1973; Mendel et al., 1991; Endrizzi et al., 1995; Ficner et al., 1995). The possibility of linkage between the functions of DCoH is suggested by the finding that a homologue (PhhB) in *Pseudomonas aeruginosa* possesses dehydratase activity and also mediates expression of an operon including its own gene and the *phhA* gene encoding phenylalanine hydroxylase (Zhou et al., 1994).

The X-ray crystal structure of tetrameric rat DCoH showed that the 104-residue monomer is an α/β protein containing an antiparallel four-stranded β-sheet flanked by three α helices (Endrizzi et al., 1995; Ficner et al., 1995; Kim & Burley, 1995). The arrangement of secondary structural elements, but not the connectivity, is similar to that seen in several classes of DNA- and RNA-binding proteins. The DCoH homotetramer contains a pair of large saddle motifs with structural similarities to the TATA-binding protein (TBP). Clefts adjacent to the saddles were proposed on the basis of sequence identities among DCoH homologues and complementarity to pterin ligands to form the dehydratase active sites.

To directly locate the active site, define the mode of pterin recognition, and explore the possibility of conformational changes due to pterin binding, we determined the high-resolution X-ray crystal structures of the free enzyme and its complex with the product analogue 7,8-dihydrobiopterin (7,8-BH_2; Fig. 1B and Kinemage 1). These structures confirm the proposed location of the active site and restrict proposals for the catalytic mechanism. Pterin binding causes only localized changes in the conformation of the protein, but the bound ligand directly alters the shape and electrostatic potential at the margins of the saddle.

Results

To reliably determine the mode of inhibitor binding and to better observe any conformational changes due to ligand binding, the X-ray crystal structure of free DCoH was extended from 3.0 Å to 2.3 Å resolution (Table 1). The current model contains 792 amino acids in eight monomers and 227 water molecules in the crystallographic asymmetric unit. The model conforms well to ideal bond lengths and angles, and has a crystallographic R value of 0.175. Compared with the initial structure of unliganded DCoH refined against data to 3.0 Å resolution (Endrizzi et al., 1995), the RMS shift was 0.51 Å for main-chain atoms and 1.7 Å for all protein atoms.

Table 1. *Data collection and refinement statistics*

	Free DCoH	7,8-BH_2 complex
Resolution	20–2.3 Å	20–2.3 Å
Unit cell dimensions (Å)	$a = b = 105.65$, $c = 196.23$	$a = b = 105.64$, $c = 196.17$
Reflections (unique/measured)	43,794/310,522	45,971/312,481
Completeness (overall/2.45–2.3 Å)	75%/33%	78%/39%
R_{merge}[a]	0.072	0.057
I/σ (overall/2.45–2.3 Å)	12/2	11/2
R_{cryst}[b]	0.175	0.174
RMS Δ bond lengths	0.012 Å	0.011 Å
RMS Δ bond angles	2.4°	2.3°
RMS Δ B (Å^2)	7.4	6.9

[a] $R_{merge} = \Sigma|I - \langle I\rangle|/\Sigma I$.
[b] $R_{cryst} = \Sigma|F_{obs} - F_{calc}|/\Sigma F_{obs}$.

Structure description

As reported on the basis of lower-resolution structures (Endrizzi et al., 1995; Ficner et al., 1995), DCoH is a tetramer of chemically identical subunits arranged with approximate 222 symmetry (Fig. 2A). The elements of secondary structure in each subunit occur in the order $\alpha\beta\beta\alpha\beta\beta\alpha$ (Fig. 2B and Kinemage 1), with the lowest overall crystallographic B values in the second α-helix (H2) and the third β-strand (S3). Although H2 and S3 form one edge of the monomer, the apparent low mobility of these segments is consistent with their extensive intersubunit contacts.

The tetramer contains two distinct types of subunit interfaces. One interface, termed the dimer interface, contains two roughly antiparallel H2 helices and juxtaposed β-strands (Fig. 2C). This pairing produces a continuous eight-stranded antiparallel β-sheet that forms a striking molecular saddle (Fig. 2D) similar to the saddle motif in TBP. The hydrophobic core under the saddle motif contains a continuous arch of six aromatic residues, three from each subunit. This arch covers two Trp 66 residues and bridges the dimer interface from one presumptive active site to the other (Fig. 2D). Side chains from the antiparallel β-sheet also contribute to the hydrophobic core. The clefts proposed to form the dehydratase active sites occur in the dimer interface (Endrizzi et al., 1995; Ficner et al., 1995).

Tetramerization is mediated by an up-and-down, X-type, four-helix bundle made up of interacting pairs of antiparallel H2 helices (Endrizzi et al., 1995; Ficner et al., 1995). This helical "tetramer interface," in contrast to the dimer interface, is comprised predominately of polar residues, and it is relatively poorly packed (Fig. 2E). Only one hydrophobic residue of the H2 helix, Leu 55,

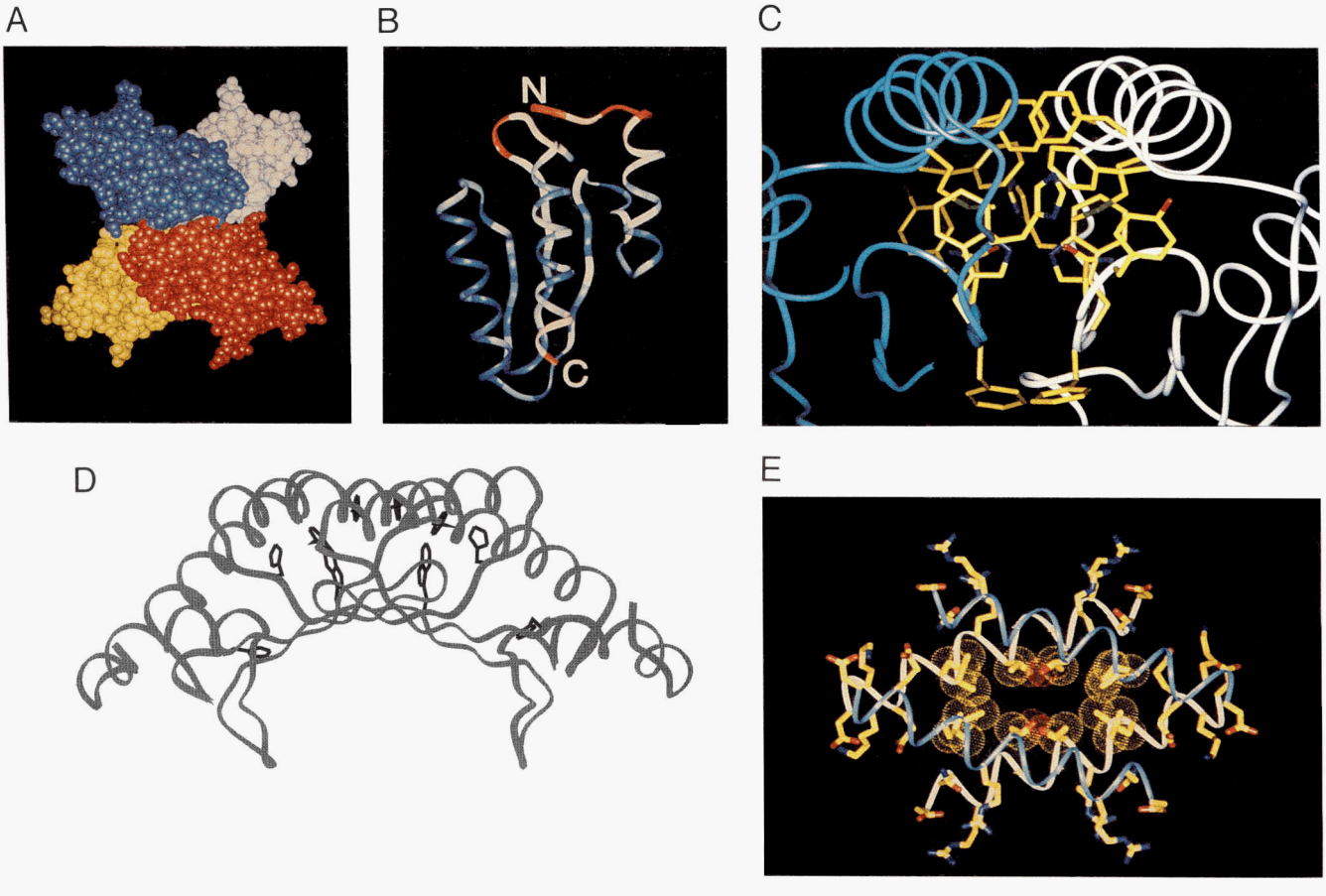

Fig. 2. DCoH structure. **A:** Space-filling drawing of the tetramer structure with the individual subunits colored white, blue, red, and yellow. View along one twofold rotation axis shows the 222 symmetry of the molecule. **B:** Ribbon diagram showing the arrangement of secondary structure elements ($\alpha\beta\beta\alpha\beta\beta\alpha$) in the monomer. Colors indicate the average main-chain B values in the eight crystallographically independent monomers. Blue, $B < 20$ Å^2; white, $B = 20$–50 Å^2; and red, $B > 50$ Å^2. Termini and loops comprising residues 6–10, 79, 80, and 104 are the most disordered regions. **C:** The dimerization interface. A twofold symmetry axis runs vertically through the middle of the figure. The antiparallel H2 helices and S3 strands from adjacent monomers (blue and white ribbons) contribute side chains (stick representation; yellow for carbon, blue for nitrogen, and green for sulfur atoms) to a well-packed hydrophobic core. The H2 helices (top, residues 43–60) contribute the side chains of Phe 43, Phe 47, Ala 54, and Met 50, with Phe 43 and Phe 47 forming an i, $i + 4$ ring–ring interaction that buries four phenyl rings between each pair of H2 helices. β-Strand S3 and the adjacent loops contribute His 63, Trp 66, Asn 68, and Tyr 70 to the dimer interface. The solvent-exposed Phe 67 side chains from each S3 also pack together in the saddle (bottom). **D:** Side view of the saddle-forming dimer emphasizing the aromatic arch containing Phe 43, Phe 47, His 63, Trp 66, and His 80, and the equivalent residues in the adjacent subunit. **E:** The tetramerization interface is formed by the H2 helix of each subunit forming a four-helix bundle. The main-chain ribbon is colored white for one dimer and blue for the second dimer. The van der Waals surfaces of Thr 51 and Leu 55 are shown to illustrate one of the cavities in the tetramer interface.

is buried in the tetramer interface. The solvent-accessible surface calculated with a 1.4 Å probe reveals internal cavities between helices from opposing saddle-forming dimers, with cavities near Gly 48, Thr 51, and Ala 54. Lys 59 lies near Glu 58 and Asp 61 at the C terminus of the adjacent H2 helix, forming favorable ionic interactions across the tetramer interface. Other charge–charge interactions between saddle dimers include 4-Å contacts between the side chains of Lys 41 and Arg 45 of one saddle-forming dimer and Arg 52 of another. Within a monomer, Arg 45 forms an ion pair with Asp 42, which caps the N terminus of the H2 helix.

In summary, the tetramer is built up via antiparallel interactions between secondary structural elements. The intersubunit contacts can be described in terms of a saddle-forming dimer interface that displays efficient packing and a more loosely packed tetramer interface that positions dimers at an approximate 90 degree orientation to one another.

Variations between molecules

The asymmetric unit of the DCoH crystals contains two independent tetramers. This affords eight independent views of the monomer, allowing analysis of structural differences resulting from crystal packing forces. The monomers superimpose with an average RMS deviation of 1.09 Å for the whole structure and 0.69 Å for main-chain atoms.

The differences in monomer conformations occur mainly at the chain termini and the "stirrups" of the saddle. Each stirrup is formed by a loop (residues 28–32) connecting β-strands one and two. Four of the stirrup loops make close intermolecular contacts in the crystals. Differences in the stirrup conformations cause the four independent saddles to vary in width from 24 to 27 Å (measured between C_α atoms of Gly 30 residues).

In addition to the ~3-Å variation in saddle width, the side chains of Arg 21, Phe 35, Gln 37, His 39, His 74, and His 80 adopt different rotamers in the eight independent monomers. Four of these conformationally variable residues occur in the saddle, suggesting that the saddle surface has a degree of plasticity. A major difference in the crystal contacts of the two independent tetramers is the packing of an H1 helix from one tetramer into a saddle of the neighboring molecule.

Structure of the 7,8-BH_2 complex

X-ray diffraction data to 2.3 Å resolution were collected from crystals of DCoH in the presence of the product analogue 7,8-dihydrobiopterin (7,8-BH_2; Fig. 1B; Kinemage 1; Table 1). The bound pterin was apparent in the electron density map calculated using phases from a ligand-free model (Fig. 3A). Refinement of the 7,8-BH_2 complex yielded a model with good geometry and stereochemistry and a crystallographic R value of 0.174 (Table 1). Despite variations in the electron density and B values, the eight crystallographically independent inhibitor molecules clearly make similar contacts with DCoH.

A 7,8-BH_2 molecule is bound in each of the four clefts in the tetramer (Fig. 4) proposed previously to form the active sites (Endrizzi et al., 1995; Ficner et al., 1995). Each cleft borders the dimer interface and contains residues from both monomers of the saddle-forming dimer. The conserved residues His 62, His 63, and Pro 64 line the active site. Other residues in the cleft include Asp 61, and loops including residues Leu 78-Glu 81 and Val 69′-Tyr 70′ of the adjacent monomer. To form the active site, Asp 61, Ala 83, and Tyr 70′ adopt a left-handed helical conformation. The 7,8-BH_2 molecule binds deep in each active site, within the arch of aromatic residues that extends through the dimer interface (Fig. 2D).

Enzyme–ligand contacts

The refined model for the 7,8-BH_2/DCoH complex shows the product analogue in position to make at least six hydrogen bonds with protein groups (Fig. 3B and Kinemage 1; Table 2). The His 63 side chain, which is nearly coplanar with the 7,8-BH_2 ring system, makes a 2.6-Å contact with N8 of the ligand. The amide nitrogen of His 63 can form a hydrogen bond with N1. Atom N2 of 7,8-BH_2 is within hydrogen bonding distance of the carbonyl oxygens of Ser 78 and His 63, and O4 forms hydrogen bonds with the main-chain amides of His 80 and Glu 81. N5 and C4a, the site of the labile proton and hydroxyl substituents of the substrate, are 5.3 Å and 4.5 Å, respectively, from Nδ1 of His 62. In addition, His 62 forms an apparent salt bridge with buried Asp 89 (2.7 Å between His 62 Nε2 and Asp 89 Oδ1). Of the atoms in the 6-dihydroxypropyl moiety, only O9 is near the protein, with a 3.4-Å contact with the side chain of Asp 61. Although residues from an adjacent monomer contribute to the active site cleft, no side chains from the neighboring subunit come within 4 Å of the bound 7,8-BH_2.

The cleft is large enough to accommodate water even in the presence of 7,8-BH_2. The arrangement of bound solvent molecules in the vicinity of the ligand, however, is not uniform in the eight independent active sites. The conformation of the conserved His 80 also shows variability, suggesting considerable flexibility in its orientation. In four of the eight active sites, the His 80 side chain lies 4.8 ± 0.4 Å from C4a of 7,8-BH_2. In the other monomers, the His 80 side chain is rotated toward the solvent, away from the ligand. Although the B-values of the His 80 side chains are relatively high in both orientations, omit maps (not shown) have clear electron density for the assigned rotamers. Nearly all contacts of 7,8-BH_2 are with conserved residues in DCoH.

Conformational changes

Binding of 7,8-BH_2 induces little conformational change in DCoH (Fig. 4 and Kinemage 1). The differences between monomers within an asymmetric unit of the free DCoH enzyme are generally greater than the differences between individual subunits with and without inhibitor.

Superimposing the liganded and unliganded active sites shows that the loop containing His 80 moves toward the ligand, and the imidazole ring of His 62 rotates slightly (Fig. 4A and Kinemage 1). Although 7,8-BH_2 binds adjacent to the saddle, almost no effect is seen on the conformation of the saddle (Fig. 4B and Kinemage 1). However, because the active sites flank the saddle, the atoms O4, C4a, N5, C6, and the 6-dihydroxypropyl of the ligand are exposed to solvent and form a composite protein/ligand surface. Thus, binding of 7,8-BH_2 changes the surface properties at the margins of the saddle (Fig. 5).

Discussion

7,8-BH_2 binding and location of the active site

The high-resolution crystal structure of the 7,8-BH_2/DCoH complex addresses four main questions: Where is the dehydratase active site? How is the pterin recognized? What conformational changes

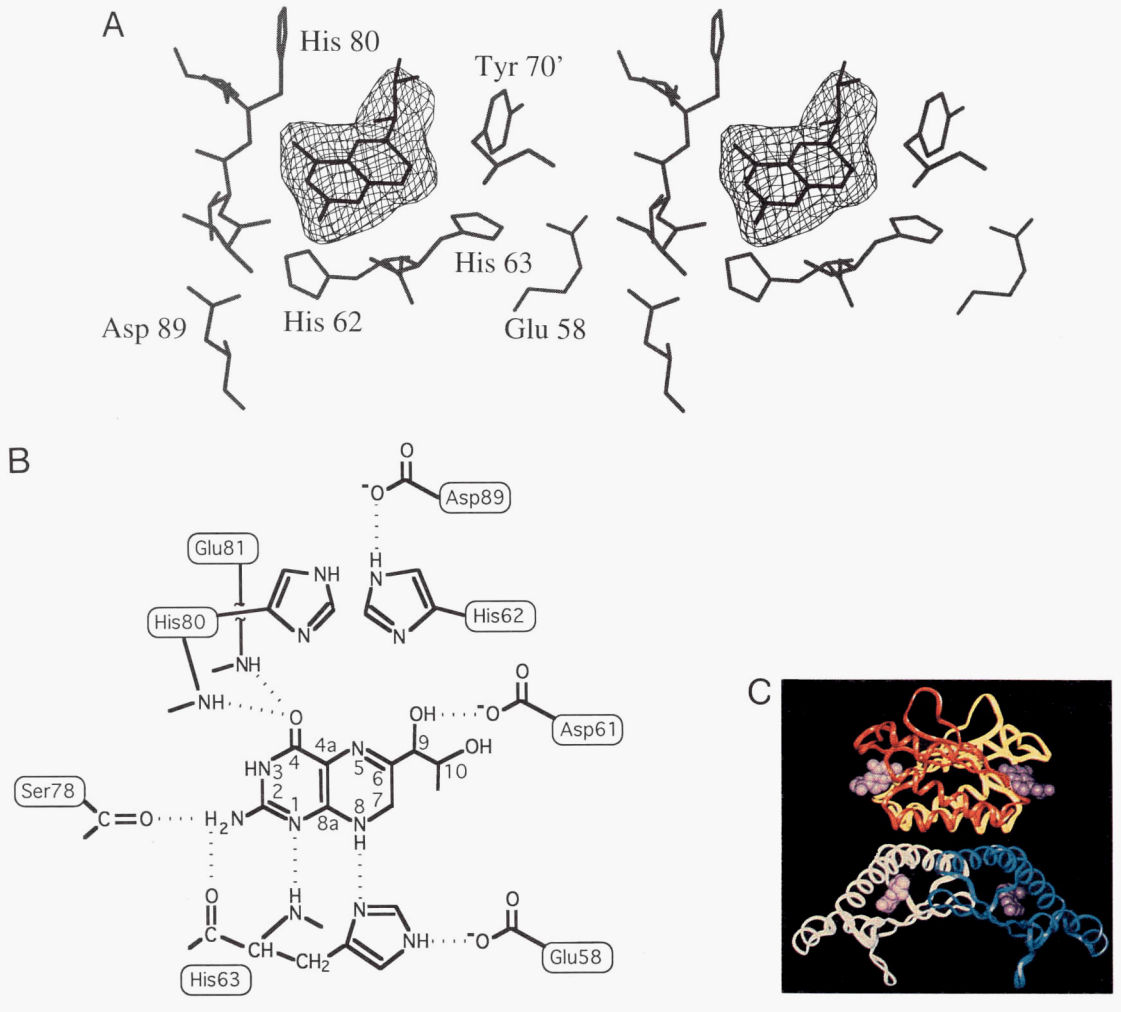

Fig. 3. Binding of the product analogue, 7,8-BH_2. **A:** Stereo view of the difference electron density map ($F_o - F_c$, 2.3 Å resolution) for 7,8-BH_2 with phases and calculated Fs obtained from the model with the active site empty. The density (contoured at 3σ) clearly indicates the location of the bound ligand. **B:** Schematic diagram showing the presumptive hydrogen bonds (dashed lines) between DCoH and 7,8-BH_2. Contact distances are summarized in Table 2. His 80 and His 62 are above and below the plane of the pterin, respectively, and do not contact each other. The pterin ring numbering system is indicated on the 7,8-BH_2 molecule. **C:** The DCoH/7,8-BH_2 complex, with ligand molecules rendered in purple space-filling atoms and the main chain of the individual subunits shown as white, blue, red, and yellow ribbons. The active site of DCoH is on the edge of the saddle motif.

accompany pterin binding? How is the dehydration reaction catalyzed? The inhibitor 7,8-BH_2 resembles the product of the dehydratase reaction catalyzed by DCoH (Fig. 1). Inhibition constants of approximately 1 μM have been reported for the true quinoid dihydropterin products (Rebrin et al., 1995), but these compounds are chemically unstable in aqueous solution and are not well suited for conventional crystallographic studies of binding. A variety of more stable pterin compounds, including 7,8-BH_2, bind DCoH with weak to moderate affinities. Based on direct and indirect measurements, reported dissociation constants of 7,8-BH_2 range from 20 μM to >200 μM (Köster et al., 1995; Rebrin et al., 1995). The origins of these differences in reported affinity are not readily identified.

The report of weak binding leaves open the possibility that 7,8-BH_2 binds DCoH differently than true substrates or products. Nonetheless, the structure of the DCoH/7,8-BH_2 complex is consistent with expectations based on less direct experiments. Under the conditions of the crystal soaks (10 mM 7,8-BH_2, 1.6 M am-

Table 2. *Protein contacts with 7,8-BH_2 ligand*

Contact (protein···7,8-BH2)	Average distance[a] (Å)
Asp 61 Oδ1···O9	3.38 ± 0.42
His 62 Nδ1···C4a	4.47 ± 0.78
His 62 Nδ1···N5	5.31 ± 0.51
His 63 NH···N1	2.91 ± 0.20
His 63 Nδ1···N8	2.62 ± 0.08
His 63 O···N2	3.03 ± 0.28
Ser 78 O···N2	2.78 ± 0.34
His 80 NH···N3	3.17 ± 0.35
His 80 NH···O4	3.08 ± 0.94
Glu 81 NH···O4	3.40 ± 0.26

[a] The average and standard deviation were calculated from the eight independent active sites in the asymmetric unit.

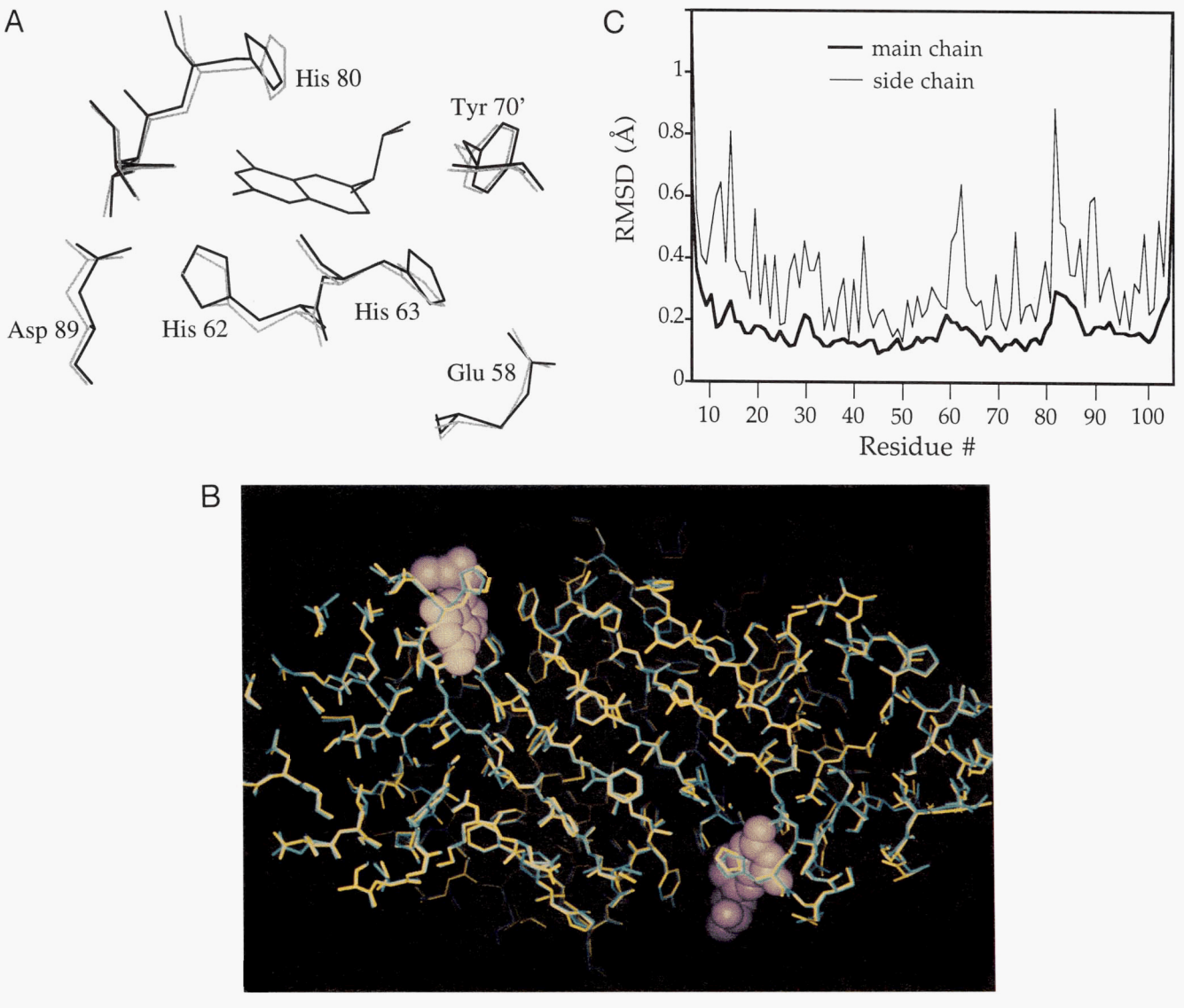

Fig. 4. Binding of 7,8-BH_2 causes small changes in the structure of DCoH. **A:** Active site region, with the free DCoH structure shown in thick bonds, the liganded structure in lighter, thin bonds, and the 7,8-BH_2 molecule in gray bonds. The largest shifts occur in the loop containing His 80. **B:** Superposition of the free enzyme (blue) and the 7,8-BH_2 complex (yellow) showing a top view of the DCoH saddle. The ligand molecules are at the upper left and lower right. **C:** Shift plot showing the average changes in atomic positions that accompany 7,8-BH_2 binding. Main-chain shifts are shown with a thick line, and side-chain shifts are shown with a thin line. The RMS coordinate shift on 7,8-BH_2 binding was 0.32 Å for backbone atoms of all eight monomers in the asymmetric unit. The apparent movement of the stirrups (residues 28–30) and the chain termini may be a consequence of the mobility of these segments in the crystals (Fig. 2B). The His 80 loop and residues surrounding Asp 61 undergo significant movements upon inhibitor binding.

monium sulfate, pH 7.5), the ligand is bound in four clefts previously inferred to form the dehydratase active sites (Endrizzi et al., 1995; Ficner et al., 1995). Each cleft contains residues His 62, His 63, Pro 64, His 80, and Asp 89, which are conserved in all DCoH homologues. Mutations of these amino acids reduce or eliminate dehydratase activity, consistent with key roles in the catalytic mechanism (Johnen et al., 1995). In addition, a Cys 82 Arg mutation just outside the cleft reduces dehydratase activity (Johnen et al., 1995; Köster et al., 1995). Replacement of Cys 82 could influence interactions with substrate and/or the positions of neighboring residues (Ser 78, His 80, and Glu 81) that make contacts with the pterin. The 6-dihydroxypropyl group of the bound ligand makes only one contact with the protein and points toward the solvent, consistent with the small effects of 6-substituents on catalytic efficiency (Lazarus et al., 1983; Rebrin et al., 1995).

In addition to the distinctive electron density for the 6-dihydroxypropyl group, the presumptive hydrogen bonds to the protein support the placement of the inhibitor. The exocyclic O4 of 7,8-BH_2 is within hydrogen bonding distance of two main-chain amides, and the exocyclic amino group forms hydrogen bonds to two main-chain carbonyls (Table 2; Fig. 3). This pairing of hydrogen-bond donors and acceptors would be eliminated if the 7,8-BH_2 molecule was flipped over in the active site.

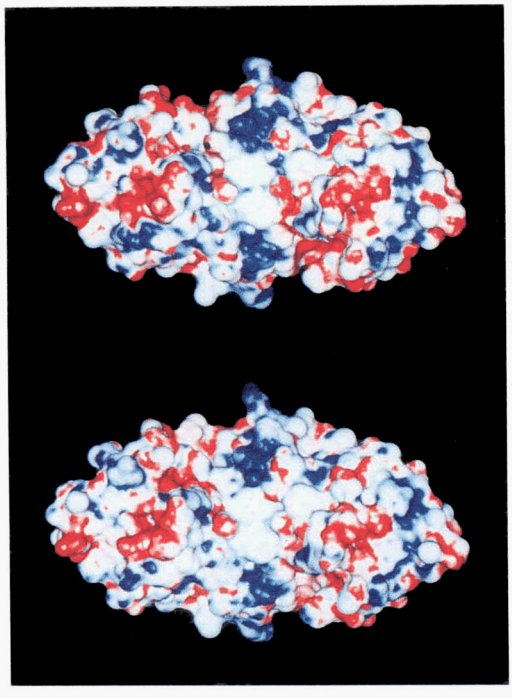

Fig. 5. Electrostatic potential displayed on the solvent-accessible surface of a DCoH saddle-forming dimer for free (top) and 7,8-BH_2-liganded DCoH (bottom). The figure was generated with Insight II (Molecular Simulations Inc.) using a 1.4-Å probe radius. Electrostatic surface potentials are colored as follows: red, −5 kT; white, neutral; blue, +5 kT. The saddle, which encompasses the middle third of the molecule (between the red stirrups) in this view, shows differences including less positive electrostatic potential compared with the saddle of TBP (Nikolov & Burley, 1994). Although 7,8-BH_2 binding induces little conformational change in DCoH, the surface and the electrostatic potential are altered at the margins of the saddle.

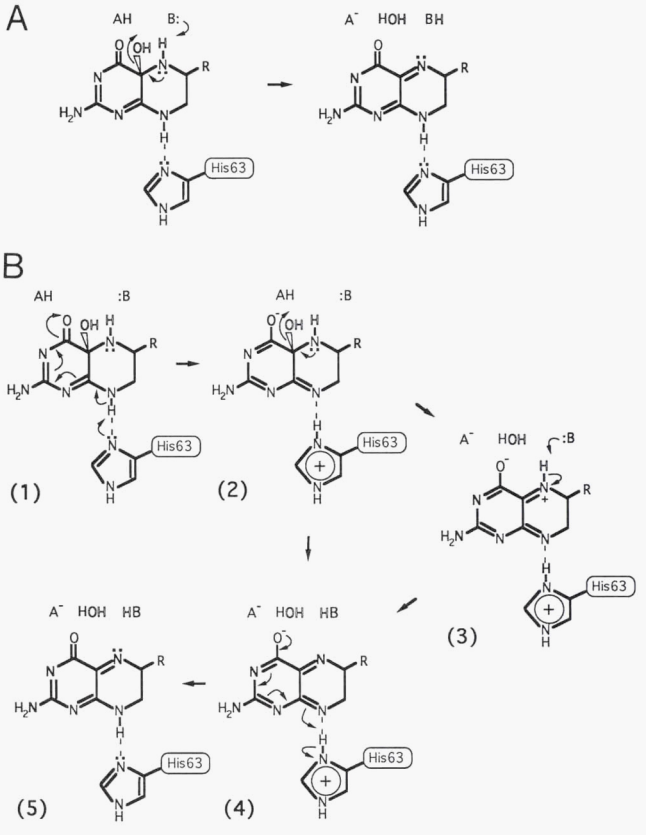

Fig. 6. Schematic of the proposed dehydratase mechanisms based on the structure of the DCoH/7,8-BH_2 complex. **A:** Elimination of water from a neutral reactant. Proton donation to the hydroxyl leaving group and proton abstraction from N5 may occur in a stepwise (not shown) or concerted mechanism. **B:** Elimination of water from an anionic reactant. Four proton transfers lead to dehydration of the substrate. His 63 abstracts the proton on N8 of the pterin ring (1), leading to the formation of an anionic species (2). An acidic group (AH: His 62, His 80, or water) donates a proton to the hydroxyl leaving group, the imine (3) deprotonates to yield the anionic product (4), and N8 is protonated to yield the neutral product (q-BH_2) (5). The general acid (HA) and general base (B) could correspond to the same chemical groups, and the dehydration steps can be stepwise or concerted. His 62 occurs on the same side of the ring as the N5 proton, supporting a role as a general base.

Dehydratase mechanism

Enzyme-catalyzed, metal-independent dehydratase reactions commonly occur by general-acid/general-base mechanisms (Sayer et al., 1973). Acid catalysis entails initial loss of the hydroxyl group to form a carbonium-ion intermediate. In contrast, base catalysis proceeds by abstraction of the labile proton and formation of an anionic intermediate. Both general acid and general base catalysis also can promote concerted eliminations. Due to the high pK_a's of carbinolamine nitrogens, most nonenzymatic dehydrations of carbinolamine compounds are proton- or general-acid-catalyzed (Jencks, 1969). In the nonenzymatic dehydration of pterin-4a-carbinolamine, however, modest rate increases and general base catalysis are observed between pH 8.4 and 11.5 (Bailey et al., 1995). This behavior may be due to resonance stabilization of the anion formed when pterin-4a-carbinolamine is deprotonated.

The binding of 7,8-BH_2 to DCoH supports mechanistic proposals in which His 62 and/or His 80 act as general-acid/general-base catalysts (Fig. 6). The reaction may proceed from neutral or anionic reactants, and loss of the elements of water can be concerted or stepwise. The simplest mechanism is a concerted elimination from the neutral substrate (Fig. 6A). In this scheme, the conserved Asp 89–His 62 dyad and His 80 are poised to accelerate the dehydration steps, and His 63 serves to position the substrate.

The DCoH structure also is compatible with a reaction mechanism suggested by Ayling and coworkers for the nonenzymatic dehydration of the anionic pterin (Bailey et al., 1995). This scheme involves four proton transfers (Fig. 6B). To form the anionic reactant, His 63 abstracts the N8 proton on the opposite side of the pterin from the constituents of water removed in the reaction. The His 63 imidazole nitrogens are within 2.7 Å of N8 and 2.9 Å of partially buried Glu 58. The interaction with Glu 58 may enhance the basicity of His 63 and position the imidazole ring in the active site. Abstraction of the N8 proton promotes formation of an oxyanion, with the negative charge on the exocyclic O4 stabilized by hydrogen bonds to the main-chain amides of His 80 and Glu 81. The negative charge at O4 promotes a facile, general-acid-catalyzed loss of the 4a-hydroxyl group. Protonation of the hydroxyl leaving group may be accomplished by the conserved His 62 (which is hydrogen bonded to the buried Asp 89) or His 80 (which is not well localized in the 7,8-BH_2 complex). Similarly, His 62 or His 80 may abstract the N5 proton, which would be expected to be relatively acidic in the zwitterion. To complete the reaction, His 63 protonates N8 to generate the neutral product.

Both proposed mechanisms assign plausible roles to all the groups that contact the inhibitor and to all the conserved residues in the active site. Most importantly, the pivotal roles of the conserved His 63 are rationalized. The function of His 63 as a general base (Fig. 6B) parallels the proposal that abstraction of the N8 proton could account for the base catalysis observed at pH $\geq$ 8.4 in the nonenzymatic dehydration reaction (Bailey et al., 1995). A catalytic function for His 63 also is supported by the absolute conservation of this residue in DCoH homologues and the finding that mutations of His 63 inactivate DCoH (Johnen et al., 1995). In addition, proton abstraction and hydrogen bonding between His 63 and N8 may inhibit the rearrangement reactions that lead to formation of 7-substituted pterins in the uncatalyzed reaction.

The structure of the 7,8-BH_2 complex also suggests specific roles for the main-chain carbonyls of Ser 78 and His 63 and the main-chain amides of His 63, His 80, and Glu 81 in positioning the substrate in the active site. In a manner analogous to the oxyanion hole in the pancreatic serine proteases, the main-chain amides that form hydrogen bonds with O4 may stabilize a pterin-oxyanion intermediate.

Owing to the differences in geometry of the true substrate, the 7,8-BH_2 complex does not allow certain identification of the acidic and basic groups that directly promote the loss of the elements of water from the pterin-4a-carbinolamine. In the substrate, the 4a position is tetrahedral (not trigonal) and the pyrazine ring is less planar. As a result, the distances observed between Nδ1 of His 62 and the C4a and N5 atoms of 7,8-BH_2 may differ significantly in the true ES complex. The inactivation of DCoH by mutations of the conserved residues Asp 89 and His 62 (Johnen et al., 1995) argues indirectly that the Asp 89-His 62 dyad may function as a general acid, a general base, or both (Fig. 6). Available data do not rule out the possibility that His 80, which also is conserved in every DCoH homologue, plays a role as proton donor or acceptor. Mutations of His 80, however, reduce activity much less than mutations at His 62 (or His 63) (Johnen et al., 1995), and His 80 is flexible in the bound and free enzymes. Consequently, His 80 may simply help position the bound substrate.

Either mechanism can be reconciled with the reported equivalent rates of dehydration of R- and S-4a-carbinolamine substrates (Rebrin et al., 1995). The unusual lack of stereospecificity implies that the rate-limiting step involves interactions with an achiral center (N8 or N5) or the participation of distinct proton donors or acceptors in the reactions of the alternate enantiomers. Alternatively, the R- and S- substrates may bind differently in the active site. The resolution of this puzzle will require studies of additional ligand complexes to further clarify the modes of binding of substrates, intermediates and transition states.

Comparison to other pterin-binding proteins

The structures of a number of proteins that bind pterins have been determined, but structural information on pterin binding is limited. Dihydrofolate reductase (DHFR) catalyzes reduction of dihydrofolate, which contains a pteridine group. The crystal structure of chicken liver DHFR in complex with $NADP^+$ and biopterin reveals a mode of binding unlike that of DCoH (McTigue et al., 1992). Biopterin is the fully oxidized form of the cofactor, with double bonds at both the 5–6 and 7–8 positions. Contacts between DHFR and the biopterin ligand are largely water-mediated, with water bridging between atom Nϵ1 of a Trp residue and O4 of biopterin. A glutamic acid side chain forms hydrogen bonds to both N3 and exocyclic N2 of the pterin.

GTP-cyclohydrolase (CYH) and 6-pyruvoyl tetrahydropterin synthase (PTPS) are both key enzymes in tetrahydrobiopterin biosynthesis. The structures of both proteins have been determined by X-ray crystallography (Nar et al., 1994, 1995b). In the structure of GTP-cyclohydrolase complexed with the substrate analogue dGTP, the ligand is bound by a Glu side chain in a manner analogous to biopterin recognition by DHFR (Nar et al., 1995a). The product of the reaction is dihydroneopterin triphosphate, which is the substrate for PTPS. A comparison of the structures of CYH and PTPS reveals common subunit topology and structural homology despite limited sequence similarity. Although there is no direct structural data on the binding of pterins to PTPS, analogies to CYH, analysis of the free-enzyme structure, and mutagenesis data have led to a model for substrate binding (Bürgisser et al., 1995). In this model, atoms N2 and N3 of the pterin ring are near a carboxylate side chain, and main-chain amide groups are in position to interact with N1 and O4 of the substrate.

Dihydropteridine reductase (DHPR) catalyzes the reduction of quinoid dihydrobiopterin (qBH_2), the product of DCoH. Two crystal structures of DHPR have been reported, but neither contains a pterin or pterin analogue (Varughese et al., 1992; Su et al., 1993). On the basis of the available structures, a model has been proposed for qBH_2 binding in a ternary complex (Varughese et al., 1994). In this model, the pteridine is sandwiched between the nicotinamide ring of NADH and a Trp residue. A Tyr residue, which is conserved in this class of dehydrogenases, is postulated to make an H-bond with the pterin 4-keto group.

Proteins that bind pterin compounds or guanine nucleotides often contain a carboxylate side chain that forms hydrogen bonds to the pterin N2 and N3 positions and a main-chain amide that donates a hydrogen bond to the 4-keto group (Bourne et al., 1991). By contrast, the DCoH/7,8-BH_2 complex provides evidence for two main-chain carbonyl contacts to N2 and two main-chain amide contacts to O4 (Fig. 3B and Kinemage 1). The differences may reflect the need for DCoH to bind to a particular tautomeric form of the pterin and to stabilize an anionic intermediate with a partial negative charge at O4. Our results indicate that DCoH recognizes the pterin ligand in a manner distinct from other examples of pterin-binding proteins.

Implications for HNF-1 binding and coactivator function

Although the purified enzyme forms a homotetramer, DCoH occurs in the nucleus as a 2:2 heterotetramer with HNF-1 (Mendel et al., 1991). The DCoH homotetramer structure suggests that the saddle-forming dimer may be preserved in the complex with HNF-1 (Endrizzi et al., 1995; Ficner et al., 1995). This possibility is supported by the larger hydrophobic surface area and the smaller cavities buried in the dimer interface relative to the tetramer interface (Fig. 2). Although the conformational rearrangements accompanying HNF-1 recognition remain to be characterized, the inference that the saddle-forming dimer binds HNF-1 has implications in coactivator function.

DCoH recognizes the N-terminal dimerization domain of HNF-1 (Mendel et al., 1991; Hansen, 1994). In vitro, a 32-amino acid peptide corresponding to the HNF-1 dimerization motif is sufficient to form an autonomous, helical dimer (De Francesco et al., 1991; Pastore et al., 1992) that binds DCoH with 2:2 stoichiometry (Endrizzi et al., 1995; J.D. Cronk & T. Alber, unpubl. results). A

typical and parsimonious arrangement for this heterotetramer involves the superposition of the dyads of DCoH and HNF-1 dimers (Fig. 7). In the saddle-forming dimer of DCoH, a twofold rotation axis passes through the center of the saddle and between the antiparallel H2 helices that form the tetramer interface (Fig. 2). Consequently, the DCoH structure suggests that HNF-1 may bind to the saddle or to the opposite face of the dimer.

Both models could account for the finding that HNF-1 blocks homotetramerization of DCoH (Mendel et al., 1991; Endrizzi et al., 1995). Binding in the DCoH saddle—which is wide enough (24–27 Å) to accommodate a pair of helices from the HNF-1 dimerization domain—could induce a conformational change that alters the tetramer interface. Alternatively, HNF-1 may bind directly to the H2 helices that mediate homotetramerization of DCoH. This latter possibility is supported by the similar spacings and charge complementation between Arg 45, Arg 52, and Lys 59 in the H2 helices and glutamates 11, 18, 24, or 32 of HNF-1. In either case, the HNF-1 helices must diverge over the surface of DCoH to make twofold symmetric contacts (Fig. 7).

The preference for coincident twofold rotation axes argues against binding models in which a parallel coiled coil (Nicosia et al., 1990; De Francesco et al., 1991) or kinked parallel helices (Pastore et al., 1992) lie completely within the saddle or across the H2 helices. In both of these arrangements, the twofold rotation axis of the HNF-1 dimerization domain would be perpendicular to the dyad symmetry axis of DCoH.

The alternative models in which HNF-1 binds to the saddle or the tetramer interface have different implications for the mechanism of coactivation. DCoH has been proposed to stimulate gene expression by stabilizing HNF-1 dimers and/or by bridging HNF-1 to another component of the transcriptional apparatus (Hansen & Crabtree, 1993). Binding of HNF-1 to the saddle would favor the idea that DCoH simply stabilizes HNF-1 dimers. Assuming that the DCoH saddle structure is preserved in the 2:2 complex, the proximity of the DCoH active site to the saddle (Fig. 3) could permit metabolites to influence HNF-1 binding. The small conformational change on binding of 7,8-BH_2 (Fig. 4) argues that direct interactions with active-site ligands would be necessary to modulate macromolecule binding. In contrast, if HNF-1 binds in the tetramerization interface, the saddle and the active-site clefts may be available to bridge the HNF-1/DCoH complex to other molecules. Resolution of these possibilities awaits direct characterization of the DCoH/HNF-1 complex.

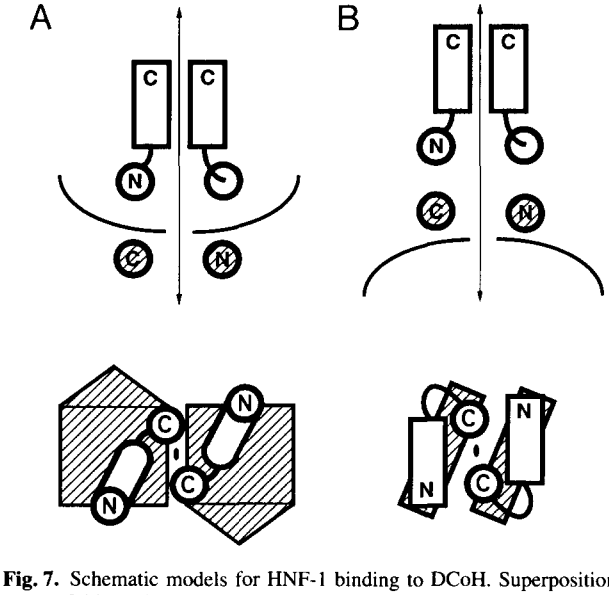

Fig. 7. Schematic models for HNF-1 binding to DCoH. Superposition of the twofold rotation axes [two-headed arrow (upper) or oval (lower)] of the saddle-forming DCoH dimer and the helical HNF-1 dimerization domain restricts the interaction to occur in (**A**) the saddle or (**B**) the tetramer interface. Views from the side (upper half) and from above the saddle (lower half) are illustrated. Helices are represented as circles (end view) or rectangles (side view), and the DCoH portion of the complex is hatched. Both of the proposed interacting surfaces of DCoH can be covered by ~14 helical residues, corresponding to approximately half of the 32-amino acid HNF-1 dimerization domain.

Materials and methods

Purification, crystallization, and ligand binding

DCoH was purified and crystallized as reported previously (Endrizzi et al., 1995). The crystals have the symmetry of space group $P3_221$, with unit cell dimensions $a = b = 105.65$ Å, $c = 196.23$ Å, $\alpha = \beta = 90°$, and $\gamma = 120°$. Native DCoH crystals were equilibrated to 1.6 M ammonium sulfate, 2% PEG 400, 100 mM HEPES, pH 7.47, prior to data collection. To collect data on the 7,8-dihydrobiopterin complex, the DCoH crystals were soaked in the same mother liquor with 7,8-BH_2 added at a concentration of 10 mM.

Data collection and processing

Data were collected at 18 °C with an R-Axis IIC image plate detector using copper K_α X-rays generated by a Rigaku rotating anode equipped with focusing mirrors. Two crystals (0.3 × 0.3 × 1 mm) were used for each data set, and each crystal was translated once along the long axis (c). Data were merged and scaled (Table 1) using the R-Axis software (Molecular Structure Corporation).

Refinement

The solvent-free DCoH model refined against the 3.0-Å resolution data (Endrizzi et al., 1995) was used as the starting point for independent refinements against data from the free protein and the 7,8-BH_2 complex. Coordinates were refined initially using the program TNT (Tronrud et al., 1987) with data from 20 to 2.3 Å, one overall B-factor, and a model for bulk solvent. Correlated B-value refinement was conducted after positional refinement converged. Electron density maps calculated with coefficients $2F_o - F_c$ and $F_o - F_c$ were inspected and adjustments were made to reduce discrepancies between the model and the electron density maps. In the later stages, water molecules were placed in peaks above 3σ in the $F_o - F_c$ maps with at least one hydrogen bond to DCoH. Rounds of model building with the interactive graphics program O (Jones et al., 1991) followed by refinement with TNT continued until no further improvements could be made to the model.

A model for the 7,8-BH_2 ligand was constructed and energy minimized using the program Insight II (Molecular Simulations, Inc.). After refinement of the free enzyme model against 20–3-Å resolution data from the 7,8-BH_2 complex, an $F_o - F_c$ electron density map phased on the native, solvent-free model was inspected. The $F_o - F_c$ map contoured at 3σ revealed unambiguous electron density for the entire inhibitor in several of the eight

dehydratase active sites. Electron density for the dihydroxypropyl group at the 6 position of the pterin in both $2F_o - F_c$ and $F_o - F_c$ maps allowed the inhibitor to be placed in the electron density. The DCoH/7,8-BH_2 complex was refined using the same strategy described above for the free enzyme. The refined model contained 792 amino acids, 8 7,8-BH_2 molecules, and 258 water molecules.

Acknowledgments

We gratefully acknowledge Dr. Georg Johnen for helpful discussions regarding the catalytic properties of DCoH and for his generous gift of 7,8-BH_2. We thank Gerald Crabtree for continuous encouragement, stimulating discussions, and review of the manuscript. This work was supported by grants to T.A. from the Keck Foundation and the NIH.

References

Bailey SW, Rebrin I, Boerth SR, Ayling J. 1995. Synthesis of 4a-hydroxytetrahydopterins and the mechanism of their nonenzymatic dehydration to quinoid dihydropterins. *J Am Chem Soc 117*:10203–10211.

Bourne HR, Sanders DA, McCormick F. 1991. The GTPase superfamily: Conserved structure and molecular mechanism. *Nature 349*:117–127.

Bürgisser DM, Thöny B, Redweik U, Hess D, Heizmann CW, Huber R, Nar H. 1995. 6-Pyruvoyl tetrahydropterin synthase, an enzyme with a novel type of active site involving both zinc binding and an intersubunit catalytic triad motif; site-directed mutagenesis of the proposed active center, characterization of the metal binding site and modeling of substrate binding. *J Mol Biol 253*:358–369.

Citron BA, Kaufman S, Milstien S, Naylor EW, Greene CL, Davis MD. 1993. Mutation in the 4a-carbinolamine dehydratase gene leads to mild hyperphenylalaninemia with defective cofactor metabolism. *Am J Hum Genet 53*:768–774.

Curtius HC, Adler C, Rebrin I, Heizmann C, Ghisla S. 1990. 7-Substituted pterins: Formation during phenylalanine hydroxylation in the absence of dehydratase. *Biochem Biophys Res Commun 172*:1060–1066.

Davis MD, Kaufman S, Milstien S. 1991. Conversion of 6-substituted tetrahydropterins to 7-isomers via phenylalanine hydroxylase-generated intermediates. *Proc Natl Acad Sci USA 88*:385–389.

Davis MD, Ribeiro P, Tipper J, Kaufman S. 1992. "7-Tetrahydrobiopterin," a naturally occurring analogue of tetrahydrobiopterin, is a cofactor for and a potential inhibitor of the aromatic amino acid hydroxylases. *Proc Natl Acad Sci USA 89*:10109–10113.

De Francesco R, Pastore A, Vecchio G, Cortese R. 1991. Circular dichroism study on the conformational stability of the dimerization domain of transcription factor LFB1. *Biochemistry 30*:143–147.

Endrizzi JE, Cronk JD, Wang W, Crabtree GR, Alber TA. 1995. Crystal structure of DCoH, a bifunctional, protein-binding transcriptional coactivator. *Science 268*:556–559.

Ficner R, Sauer UH, Stier G, Suck D. 1995. Three-dimensional structure of the bifunctional protein PCD/DCoH, a cytoplasmic enzyme interacting with transcription factor HNF1. *EMBO J 14*:2034–2042.

Hansen LP. 1994. HNF1α is post-translationally regulated by heterodimerization and protein stabilization [thesis]. Stanford, California: Stanford University.

Hansen LP, Crabtree GR. 1993. Regulation of the HNF-1 homeodomain proteins by DCoH. *Curr Opin Genet Dev 3*:246–253.

Huang CY, Kaufman S. 1973. Studies on the mechanisms of action of phenylalanine hydroxylase and its protein stimulator. (I. Enzyme concentration dependence of the specific activity of phenylalanine hydroxylase due to a nonenzymatic step). *J Biol Chem 248*:4242–4251.

Huang CY, Max EE, Kaufman S. 1973. Purification and characterization of phenylalanine hydroxylase-stimulating protein from rat liver. *J Biol Chem 248*:4235–4241.

Jencks W. 1969. *Catalysis in chemistry and enzymology*. New York: McGraw-Hill.

Johnen G, Kowlessur D, Citron B, Kaufman S. 1995. Characterization of the wild-type form of the 4a-carbinolamine dehydratase and two naturally occurring mutants associated with hyperphenylalaninemia. *Proc Natl Acad Sci USA 92*:12384–12388.

Jones TA, Zou JY, Cowan SW, Kjeldgaard M. 1991. Improved methods for building protein models in electron density maps and the location of errors in these models. *Acta Crystallogr A 47*:110–119.

Kaufman S. 1970. A protein that stimulates rat liver phenylalanine hydroxylase. *J Biol Chem 245*:4751–4759.

Kaufman S. 1993. New tetrahydrobiopterin-dependent systems. *Annu Rev Nutrition 13*:261–286.

Kim JL, Burley SK. 1995. PCD/DCoH: More than a second molecular saddle. *Structure 2*:531–534.

Köster S, Thöny B, Macheroux P, Curtius HC, Heizmann C, Pfleiderer W, Ghisla S. 1995. Human pterin-4α-carbinolamine dehydratase/dimerization cofactor of hepatocyte nuclear factor-1α: Characterization and kinetic analysis of wild-type and mutant enzymes. *Eur J Biochem 231*:414–423.

Lazarus RA, Benkovic SJ, Kaufman S. 1983. Phenylalanine hydroxylase stimulator protein is a 4a-carbinolamine dehydratase. *J Biol Chem 258*:10960–10962.

McTigue MA, Davies JF, Kaufman BT, Kraut J. 1992. Crystal structure of chicken liver dihydrofolate reductase complexed with $NADP^+$ and biopterin. *Biochemistry 31*:7264–7273.

Mendel DB, Khavari PA, Conley PB, Graves PB, Hansen LP, Admon A, Crabtree GR. 1991. Characterization of a cofactor that regulates dimerization of a mammalian homeodomain protein. *Science 254*:1762–1767.

Nar H, Huber R, Auerbach G, Fischer M, Hösl C, Ritz H, Bracher A, Meining W, Eberhardt S, Bacher A. 1995a. Active site topology and reaction mechanism of GTP cyclohydrolase I. *Proc Natl Acad Sci USA 92*:12120–12125.

Nar H, Huber R, Heizmann CW, Thöny B, Bürgisser D. 1994. Three-dimensional structure of 6-pyruvoyl tetrahydropterin synthase, an enzyme involved in tetrahydrobiopterin biosynthesis. *EMBO J 13*:1255–1262.

Nar H, Huber R, Meining W, Schmid C, Weinkauf S, Bacher A. 1995b. Atomic structure of GTP cyclohydrolase I. *Structure 3*:459–466.

Nicosia A, Monaci P, Tomei L, DeFrancesco R, Muzzo M, Stunnenberg H, Cortese R. 1990. A myosin-like dimerization helix and an extra-large homeodomain are essential elements of the tripartite DNA binding structure of LFB1. *Cell 61*:1225–1236.

Nikolov DB, Burley SK. 1994. 2.1 Å resolution refined structure of a TATA box-binding protein (TBP). *Nature Struct Biol 1*:621–637.

Pastore A, DeFrancesco R, Morelli MAC, Nalis D, Cortese R. 1992. The dimerization domain of LFB1/HNF1 related transcription factors: A hidden four helix bundle? *Protein Eng 5*:749–757.

Rebrin I, Bailey S, Boerth S, Ardell M, Ayling J. 1995. Catalytic characterization of 4a-hydroxytetrahydropterin dehydratase. *Biochemistry 34*:5801–5810.

Sayer JM, Peskin M, Jencks WP. 1973. Imine-forming elimination reactions. I. General base and acid catalysis and influence of the nitrogen substituent on rates and equilibria for carbinolamine dehydration. *J Am Chem Soc 95*:4277–4287.

Su Y, Varughese KI, Xuong NH, Bray TL, Roche DJ, Whiteley JM. 1993. The crystallographic structure of a human dihydropteridine reductase NADH binary complex expressed in *Escherichia coli* by a cDNA constructed from its rat homologue. *J Biol Chem 268*:26836–26841.

Tronrud DE, TenEyck LF, Matthews BW. 1987. TNT: TenEyck–Tronrud refinement package. *Acta Crystallogr A 43*:489–503.

Varughese KI, Skinner MM, Whiteley JM, Matthews DA, Xuong NH. 1992. Crystal structure of rat liver dihydropteridine reductase. *Proc Natl Acad Sci USA 89*:6080–6084.

Varughese KI, Xuong NH, Kiefer PM, Matthews DA, Whiteley JM. 1994. Structural and mechanistic characteristics of dihydropteridine reductase: A member of the Tyr-$(Xaa)_3$-Lys-containing family of reductases and dehydrogenases. *Proc Natl Acad Sci USA 91*:5582–5586.

von Strandmann EP, Ryffel GU. 1995. Developmental expression of the maternal protein XDCoH, the dimerization cofactor of the homeoprotein LFB1 (HNF1) *Development 121*:1217–1226.

Zhou G, Xia T, Song J, Jensen RA. 1994. *Pseudomonas aeruginosa* possesses homologues of mammalian phenylalanine hydroxylase and 4a-carbinolamine dehydratase/DCoH as part of a three-component gene cluster. *Proc Natl Acad Sci USA 91*:1366–1370.